Pharmacological and Molecular Docking studies of *Allium ampeloprasum* L.

Deepti Teotia
Chaudhary Charan Singh University Meerut
Anjali Malik
Chaudhary Charan Singh University Meerut
Vijai Malik
vijaimalik1973@gmail.com

Chaudhary Charan Singh University, Meerut

Research Article

Keywords: Allium ampeloprasum, Antibacterial activity, Antioxidant activity, GC-MS analysis, Molecular Docking, MD Simulation, MM-PBSA, PCA

Posted Date: July 16th, 2025

DOI: https://doi.org/10.21203/rs.3.rs-7126283/v1

Additional Declarations: The authors declare no competing interests.

Abstract

Objective:
To investigate the bioactive compounds present in the leaf extract of *Allium ampeloprasum* and evaluate its antioxidant and antibacterial potential using experimental and computational methods.

Methods:
The phytochemical composition of the leaf extract was analyzed using Gas Chromatography-Mass Spectrometry (GC-MS). Antioxidant activity was determined using the DPPH radical scavenging assay, while the Antibacterial activity was tested against four bacterial strains (*Pseudomonas aeruginosa*, *Staphylococcus aureus*, *Escherichia coli*, and *Bacillus subtilis*) using the well diffusion method. Molecular docking was conducted to assess the binding affinities of identified compounds with bacterial DNA gyrase, followed by Molecular Dynamics (MD) simulations, MM-PBSA (Molecular Mechanics Poisson–Boltzmann Surface Area) and PCA (Principle component analysis) to evaluate complex stability.

Results:
The leaf extract of *A. ampeloprasum* showed the strong antioxidant activity, with DPPH radical scavenging reaching up to 87.3% at 500 µg/mL, attributed to its phenolic and flavonoid content. The highest antibacterial activity was against *Bacillus subtilis* (10 mm inhibition zone at 1000 µL/mL), followed by *Escherichia coli* and *Staphylococcus aureus* (7 mm each at 1000 µL/mL concentration). GC-MS analysis revealed several bioactive compounds, among which gamma-sitosterol exhibited the strongest binding affinity to DNA gyrase (-7.1 kcal/mol), comparable to ciprofloxacin. MD simulation and MM-PBSA and Principle component analysis confirmed the stability of the gamma-sitosterol–DNA gyrase complex.

Conclusion:
The leaf extract of *A. ampeloprasum* possesses strong antibacterial and antioxidant properties due to the presence of valuable natural compounds. In India, this plant is not commonly cultivated and remains underutilized, despite offering numerous health benefits. Currently, *A. ampeloprasum* is being grown as a commercial crop in the Uttarakhand hills, Manipur, and Kashmir. Since it is growing well in the study area, it can be recommended to farmers for food value addition and for use in functional food development. This may also be important for selecting superior *Allium* genotypes with enhanced bioactive properties. While *Allium sativum* L. and *Allium cepa* L. are commonly grown species across India, the introduction of *A. ampeloprasum* in new regions could provide access to natural medicines and offer farmers new income opportunities through the cultivation of medicinal plants.

Introduction

In recent years, medicinal plants have gained significant attention as natural sources of antibacterial compounds. These natural alternatives not only help combat antibiotic resistance but also minimize the side effects associated with chemical antibiotics (Tavakkoli et al., 2015).

Genus *Allium* includes more than 1,089 accepted species (POWO, 2021) among them garlic (*Allium sativum*), onion (*Allium cepa*), leeks (*Allium ampeloprasum* var. *porrum*), chives (*Allium schoenoprasum*), and shallots (*Allium ascalonicum*) are the most utilized and studied edible species (Poojary et al., 2017). The genus *Allium* has long been recognized for its ethno pharmacological significance, owing to its diverse medicinal properties and widespread traditional use across different cultures (Teotia et al., 2024). *Allium* species offer a wide array of health benefits, including antiviral, antibacterial, antifungal, antidiabetic, anticancer, antiplatelet, antispasmodic, antiseptic, anthelmintic, antithrombotic, antiasthmatic, carminative, antioxidant, anti-inflammatory, antihypertensive, hypoglycemic, hypotensive, lithontriptic, and hypocholesterolemic effects (Najeebullah et al., 2021). Garlic, a widely studied member of the *Allium* genus, exhibits potent antimicrobial properties due to presence of bioactive compounds, including allicin, vinyldithiin, ajoene, and diallyl polysulfides (Muhsin et al., 2015). Recent studies have shown an association between reduced risk and incidence of breast cancer with the consumption of certain *Allium* species, especially *Allium sativum* and *Allium ampeloprasum* (Pourzand et al., 2016).

Allium ampeloprasum L. (Amaryllidaceae) is a monocotyledonous plant which is commonly known as broadleaf wild leek. This is a unique species, single-pod garlic which is highly valued for its medicinal properties (Dey & Khaled, 2015). Native to the Mediterranean region—including Southern Europe, North Africa, and Western Asia, it has been introduced to other parts of the world, such as North and South America and Australia, and is cultivated in various regions of Asia, including India (Guhabakshi et al., 1999). *A. ampeloprasum* possesses a range of pharmacological properties, including antitoxic, antioxidative, immunostimulatory, and anti-inflammatory effects due to the presence of many sulphur containing bio-active constituents which include: dimethyl disulphide, methyl propenyl

disulphide, propyl propenyl disulphide, dimethyl trisulfide, methyl propyl trisulfide, methyl propenyl trisulfide, S-methyl cysteine sulfoxide, S-propyl cysteine sulfoxide, S-propenyl cysteine sulfoxide and N-(γ-glutamyl)-S-(E-1-propenyl) cysteine (Dey & Khaled, 2015). *A. ampeloprasum* is recognized as a valuable source of dietary fiber, zinc, polyunsaturated fatty acids particularly linoleic acid as well as a range of lipophilic and hydrophilic bioactive compounds exhibiting significant antioxidant activity (Devi et al., 2014).

Gas Chromatography-Mass Spectrometry (GC-MS) is a crucial analytical technique for characterizing the complex chemical composition of plant extracts. This method allows for the identification and quantification of a broad spectrum of bioactive compounds, providing a detailed chemical profile of the plant (Jain et al., 2024).

DNA gyrase, a type II topoisomerase, is a key enzyme that has been used as a target in molecular docking studies. This enzyme introduces negative supercoils into DNA using ATP hydrolysis and is essential for bacterial survival, while being absent in higher eukaryotes (Reece & Maxwell, 1991). This make it an attractive target for antibacterial drug development. Fluoroquinolones, such as ciprofloxacin, are well-established gyrase inhibitors and are frequently used as positive controls in various *in vitro* studies (Richards et al. 1998).

Several *in vitro* and *in vivo* studies have been conducted to evaluate the antimicrobial potential of *Allium* spp. such as the methanol extracts of *Allium* were tested against a set of Gram-positive (*Staphylococcus aureus, Staphylococcus feacalis, Bacillus cereus, Enterococcus feacium and Bacillus subtilis*) and Gram-negative (*Escherichia coli, Pseudomonas aeruginosa* and *Enterobacter feacalis*) bacterial strains (Dziri et al., 2012). Bareemizadeh et al. (2014) demonstrated that ethyl acetate extracts of *A. ampeloprasum* exhibited strong antimicrobial activity against *Klebsiella pneumoniae* and *Shigella flexneri* at a concentration of 250 µg/mL, likely due to its pinene and phenol content. Caputo et al. (2022) reported that extracts from the aerial parts of *A. ampeloprasum* significantly inhibited the adhesion of *P. aeruginosa* (95.78%) and *S. aureus* (85.01%). Conversely, Añides et al. (2021) found that while *A. ampeloprasum* extracts did not inhibit *P. aeruginosa* and *B. subtilis*, they exhibited strong antibacterial effects against *E. coli*, *K. pneumoniae*, *S. typhimurium*, and *S. aureus*. The authors did not find antimicrobial activity with in-silico validation of *A. ampeloprasum* extract against *Bacillus subtilis, Escherichia coli*, *Pseudomonas aeruginosa* and *Staphylococcus aureus*. Therefore, the aim of the present study was to investigate the bioactive compounds present in the leaf extract of *A. ampeloprasum* and evaluate their antibacterial potential through well diffusion assay and antioxidant activity, molecular docking, molecular dynamics simulations and MMPBSA studies with a focus on identifying potential plant-derived inhibitors of bacterial DNA gyrase.

Material and Methods

1. Collection of Plant material

Plant sapling of *A. ampeloprasum* were collected from Bhowali station Nanital (Uttrakhand) and grown in Botanical garden of CCSU, Meerut, Uttar Pradesh (India) in the month of October 2023. Leaves of plant were harvested in month of July 2024 for experimental purpose.

1.1. Preparation of Plant extract

Samples were ground and then 2.5 gm of samples were taken and mixed with 25 ml of solvent (Absolute Methanol). Sample mixtures were incubated on a rocker shaker for 24 hours. The extracts were filter with Whatman filter 1. Then extracts were completely dried in the oven at 40°C. Extracts were collected in micro centrifuge tube and stored at 4°C. Further dilution is done by using distilled water. Five concentration of plant extracts were used for antibacterial assay i.e., 50 (µg/well), 125 (µg/well), 250 (µg/well), 500 (µg/well) and 1000 (µg/well).

1.2. Percentage yield

Percentage yield (PY) of the concentration crude extract was estimated using the formula given below:

Yield % = weight of crude plant extract x 100/ weight of powdered plant material

1.3. GC-MS analysis

The extracted plant samples were analyzed using Gas Chromatography-Mass Spectrometry (GC-MS) to identify and measure their chemical constituents. A high-resolution instrument with a fused silica capillary column, specifically the SH-Rxi-5Sil MS column (5% biphenyl and 95% dimethyl polysiloxane), measuring 30 meters in length, 0.25 mm in inner diameter, and with a 0.25 µm film thickness

was employed. The analysis was conducted at a temperature range of 320-350°C. Helium (He) was used as the mobile phase, flowing at 1.0 ml/min. The gas chromatography process started at 50°C and increased to 300°C at a rate of 5°C/min. A 1 microliter injection volume was used. Samples dissolved in methanol, were analyzed within a mass-to-charge ratio (m/z) range of 50-650. The results were compared using an integrated chemical library search program that identified individual compounds based on their retention times and mass spectra. Peak integration and area normalization quantified the relative abundance of each compound in the sample.

1.4. Total Phenolic Content (TPC)

TPC was estimated using Folin-Ciocalteu Colorimetric method of Aiyegroro & Okoh, (2010) with slight modification. 2.5 mL of freshly synthesized Folin-ciocalteu reagent (10%) was poured into test tube containing 1 mL of plant extract. 2 mL Na_2CO_3 (2%) was then added to the test tube and kept under the dark conditions for 30 minutes. Absorbance was noted at 765 nm using UV-Vis Spectrophotometer (Shimadzu-80228), Japan.

Gallic acid (1mg/mL) was used as standard and five concentrations (20-100 µg/mL) were used for preparing standard curve. 1mL solvent along with 2.5 mL Folin-Ciocalteu reagent and 2mL Na_2CO_3 solutions was used as blank. Experiment were performed in triplicates and TPC was calculated using the calibration curve ($y=0.0119x + 0.2346$, $R^2 =0.998$).

TPC in plant extracts was calculated by the formula given below and expressed in mg Gallic Acid Equivalent (GAE)/gm

$T = C \times V/M$

Here,

T = Total Phenol Content mg/gm GAE

C = Concentration of Gallic Acid obtained from the calibration curve in mg

V= Volume of plant extract in mL

M = Weight of plant extract in gm

1.5. Total Flavonoid Content (TFC)

TFC was estimated using Aluminium Chloride Colorimetric method used by Aiyegroro & Okoh, (2010) with minor modifications. 0.3mL aluminium chloride (10%) and 0.3mL potassium acetate (1M) were poured in a test tube containing 1 mL of plant extract. 3mL of methanol and 3.5mL of distilled water was taken and then added to the test tube. This was kept under dark conditions for 30 minutes. Absorbance of the solution was noted at 417 nm.

Quercetin (1mg/mL) was considered as reference compound and standard curve was prepared using five concentrations (20-100 µg/mL). All the experiment was performed in triplicates and the mean value was used for further calculations. The calibration curve ($y=0.0188x+0.1532$, $R^2+0.9993$) was used to calculate the TFC of the plant extracts.

TFC of the plant extract was calculated using the formula given below. TFC was expressed in mg/gm of Quercetin equivalent (mg QE/g).

$T + C \times V/M$

Here,

T = Total Flavonoid Content mg/gm Quercetin Equivalent (QE)

C = Concentration of Quercetin obtained from the calibration curve in mg

V= Volume of plant extract in mL

M = Weight of plant extract in gm

1.6. Antioxidant Activity

Each sample was dissolved in 95% methanol to make a concentration of 1 mg/ml and then diluted to prepare the series concentrations for antioxidant assays.

1.6.1. DPPH Assay

The free radical scavenging activity of the fractions was measured in vitro by 2,2 - diphenyl-1-picrylhydrazyl (DPPH) assay according to the method described as Brand-Williams et. al., (1995). A 0.1 mM DPPH solution was prepared in methanol. Plant samples at five varying concentrations (20-100 µg/mL) were mixed with the DPPH solution in a 1:1 ratio and incubated in the dark for 20–30 minutes. Absorbance was measured at 517 nm using a spectrophotometer. DPPH mixed in methanol solvent was taken as control. Ascorbic acid was used as standard. Lower absorbance indicates higher activity. IC50 values can be determined for comparative analysis. Antioxidant activity was calculated as % inhibition of DPPH using the formula:

% Inhibition = (Abc – Abs)/ Abc x 100

Here,

Abc is Absorbance of Control

Abs is Absorbance of Sample (Standard / plant extract)

1.6.2. IC_{50} value

IC_{50} is the concentration of the plant extract/standard required to scavenging 50% of the free radicals. This value is inversely related to the antioxidant capacity as lower the IC_{50} values higher is the antioxidant capability and vice-versa. The value was calculated using the formula **y = mx+b;** which was obtained by plotting the graph between the concentration and % inhibition recorded in the DPPH assay.

2. Antimicrobial studies

Antimicrobial efficacy for the plant extracts was assessed using four aforementioned bacterial strains. Well diffusion assay was used to determine the zone of inhibition (ZOI) of the plant extract (Bauer et al., 1966).

2.1. Bacterial Strains

Bacterial strains used in the present investigation were *Bacillus subtilis* (MTCC-2057), *Escherichia coli* (MTCC-41), *Pseudomonas aeruginosa* (MTCC-2453) and *Staphylococcus aureus* (MTCC-96) were obtained from Microbial Type Culture Collection and Gene Bank (MTCC), Institute of Microbial Technology Chandigarh.

2.2. Bacterial culture

Bacterial strains were cultured in nutrient agar procured from Hi-media. About 28 gm of nutrient agar powder was mixed in 1000 mL distilled water followed by autoclaving for 20 minutes at 121^{o} C and 15 psi pressure. A loopful of lyophilized bacteria (powdered form) was streaked on the solid and sterilized nutrient agar plates. Streaked bacterial plates were incubated for 24 hours in B.O.D incubater shaker at 37^{o} C for 24 hours. For experimental studies, the turbidity of bacterial cultures was checked and calibrated to standard i.e., 0.5 McFarland ($1.5x\ 10^{8}$ CFU/mL).

2.3. Well diffusion assay

To assess the antibacterial potential of the plant extracts, well diffusion assay was carried out (Bauer et al., 1996). About 28 gm of nutrient agar was mixed in 1000 mL distilled water and kept in autoclave at 121^{o} C for 20 minutes. 25 mL of sterilized nutrient agar media was poured in aseptic petri plates. 100 µL of calibrated bacterial culture ($1.5x\ 10^{8}$ CFU/mL) was evenly spread over the solidified media. 10 µL of plant extract with five different concentrations 50 (µg/mL), 125 (µg/mL), 250 (µg/mL), 500 (µg/mL) and 1000 (µg/mL) were loaded in wells and name them A, B, C, D & E respectively. Ciprofloxacin (0.1mg/mL) was used as positive control and loaded with it labelled as F. Prepared petri plates were then incubated in B.O.D at 37^{o} C for 24 hours. The ZOI obtained was measured using antibacterial scale, Himedia. The experiments were performed in triplicates and the mean value of ZOI was recorded.

3. Detailed Methodology of Molecular Docking

3.1 Library generation and protein retrieval

The 3D structure of ligands isolated from methanolic extract of *A. ampeloprasum* leaves were downloaded from PubChem database (https://pubchem.ncbi.nlm.nih.gov) in an SDF file format. It is then converted into PDBQT format by using Open Babel GUI (O'Boyle et al., 2011). The 3D protein structure of the target enzyme DNA Gyrase with PDB ID 6fju was downloaded from protein data bank i.e.., RCSB PDB (https://www.rcsb.org/) in PDB (Protein Databank) format. It was converted into PDBQT format by Autodock 4.2. (Morris et al., 2009). The protein subjected to energy minimization and optimization with the help of SPDBV, to make it stable. Now, this protein was used for performing the molecular docking process by using Autodock Vina (Morris et al., 2009).

3.2. Molecular Docking studies

The molecular docking studies of all the identified compounds and proteins were performed with AutoDock Vina (Morris et al., 2009). Receptor active site dimensions were set at -31.684 x 8.021 x -4.598 XYZ coordinates for 6fju with 0.375 grid spacing for each atom type. The box dimension was kept as 40 A^0 x 40 A^0 x 40 A^0 (Aliye et al., 2021). Ten confirmations were obtained for each docking experiment, each with a corresponding binding affinity expressed in kcal/mol. For further studies, the ligand-binding position with the lowest binding energy was selected. In our investigation, the phytochemicals that have strong interactions with target enzymes were further examined.

3.3. Visualization of Ligand-Protein interaction

The best possible 2D structures between ligand and protein were analyzed using Discovery Studio Visualizer for different interactions such as conventional H Bond, Vander wall interactions, Carbon H Bond, Pi-Alkyl, Pi-Sulphur, Pi-Sigma, Pi-Anion and Alkyl are visualized (Design et al., 2014).

3.4. Molecular Dynamics simulation

To assess the dynamic properties of the ligand-protein complexes, MD simulations were conducted. The Charmm36-feb 2021.ff force field was utilized in all simulations using GROMACS 2020.1-1 version. The ligand topology files were created using the CGenFF server (Vanommeslaeghe et al., 2010). Protein complexes that had been created were solved in a cubic box, and enough ions were added to keep the system neutral. The steepest descent approach was used to minimize the system's energy with a convergence threshold of less than 1000 kJ/mol/nm in order to remove any steric collisions among atoms. Equilibration was carried out in two stages. The solvent and ions were kept unrestrained in the NVT ensemble for 100ns in the first phase, while the restraint weight from the protein and protein-ligand complexes was gradually reduced in the NPT ensemble for 100ns in the second phase. The LINCS algorithm was used to keep all hydrogen bonds constrained. Utilizing Berendsen's temperature and Parrinello-Rahman pressure coupling, the temperature and pressure of the system were kept at 300 K and 1 atm respectively (Berendsen et al.,1984). The conformational dynamics and stability of protein–ligand complexes were analyzed using GROMACS and Python 3.8 by monitoring backbone RMSD, ligand RMSD, complex RMSD, RMSF, radius of gyration (Rg), and solvent-accessible surface area (SASA).

3.5. MMPBSA free energy calculation

MMPBSA was used to calculate the binding energy and the energy contribution per residue. In MMPBSA, the nonpolar component (ΔGnpsolv) was computed using a linear connection to the solvent accessible surface area (SASA), whereas the polar percentage of solvation energy (ΔGpsolv) was evaluated by solving the Poisson-Boltzmann equation. In this study, different parts of the binding free energy of complexes were estimated using the gmmpbsa module of GROMACS (Kumara et al., 2014). The 100ns of the trajectory were used in the analysis.

3.6. Principal Component Analysis

Principal Component Analysis (PCA) was carried out using the Galaxy server (Sloggett et al., 2013) to investigate the dynamic behavior of protein-ligand complexes. Protein conformation plays a critical role in maintaining the structural integrity required for effective binding. The covariance matrix generated during the simulation was utilized to analyze the large-scale motions within the enzyme-ligand systems. PCA is a widely accepted approach for identifying key conformational changes and assessing the flexibility of biomolecular structures. This computational strategy enabled a wide-range evaluation of the structural dynamics and energetic profiles of the protein-ligand interactions that offer valuable insights into the therapeutic potential of *A. ampeloprasum* phytochemicals.

Results

4.1. Percentage yield

The percentage yield of methanolic leaf extract from *A. ampeloprasum* was determined through an extraction process. A total of 2500 gm of powdered leaf material was used, yielding 367 mg of extract with 14.68%, recovery percentage.

4.2. GC-MS analysis

The methanol extracts of *A. ampeloprasum,* overall 23 different compounds were identified (table 1) along with their retention time and m/z value. The GC-MS chromatogram which shows peak 1 with an m/z value of 43.00, corresponding to 2- Pentanol, acetate, while peak 2, with an m/z value of 57.00, 2-(Isobutoxymethyl)oxirane. peak 3, 4, 5 and 6 with m/z 73.00, 73.00, 73.00, and 68.05 respectively, reveal the presence of Dodecanoic acid, methyl ester, Dodecanoic acid, methyl ester, Methyl tetradecanoate and Neophytadiene which are fatty acid compounds. Peak 7, 8, 9 with an m/z value 43.05, 81.05 and 81.05 are shown the presence of compound 2-Pentadecanone, 6,10,14-trimethyl- and Neophytadiene. Peak 10 and 11 with an m/z value 74.00, 73.00 indicates the compound is Hexadenoic acid, methyl ester and n-Hexadecanoic acid. Peak 12,13 and 14 with m/z value 67.00, 55.05 and 55.05 are 9,12-Octadecadienoic acid (Z,Z)-, methyl ester, 9-Octadecenoic acid, methyl ester, (E)-and 9-Octadecenoic acid (Z)-, methyl ester respectively. Peak 15 with an m/z value 71.05 is phytol, and peak 16 with an m/z value is 74.00 is Methyl stearate. Peak 17, 18, 19 with m/z value 57.00 is Hexatriacontane, Tetracosane and Tetracontane. Peak 20 with m/z value 97.10 represents octacosanol. Peak 21 with an m/z value 147.10 is beta-Sitosterol acetate, and peak 22 with an m/z value 165.00 is alpha.-Tocopherol-.beta.-D-mannoside. Peak 23, 24 and 25 with an m/z value 57.05, 239.15, 43.05 represents compounds Phytyl stearate, 16-Hentriacontanone and gamma-Sitosterol respectively. The GC-MS chromatogram of different peaks corresponding to their respective compounds are given in fig.1, table 1.

Table 1. List of Bioactive Compounds Identified through GC-MS analysis from methanolic leaf extract of *A. ampeloprasum*

S.N	Compound Name	Formula	MW	RT	Peak area	Class	Reported activity	References
1	2-Pentanol, acetate	C7H14O2	130.18	2.53	1	Carboxylic acid ester	Not found	
2	2-(Isobutoxymethyl)oxirane	C7H14O2	130.18	12.997	9.09	Glycidyl ether	Not found	
3	Dodecanoic acid, methyl ester	C13H26O2	214.34	13.695	0.54	Fatty acid ester	Antimicrobial	Reddy et al., 2018
4	Dodecanoic acid, methyl ester	C13H26O2	214.34	13.752	3.64	Fatty acid ester	Antimicrobial	Reddy et al., 2018
5	Methyl tetradecanoate	C15H30O2	242.4	16.071	3.02	Fatty acid ester	Anticancer	Ukwubile et al., 2019
6	Neophytadiene	C20H38	278.52	17.261	6.91	Diterpenes	anti-inflammatory, anti-microbial, antioxidant	Akter et al., 2024
7	2-Pentadecanone, 6,10,14-trimethyl-	C18H36O	268.48	17.335	0.5	Fatty acid	Antimicrobial	Amos-Tautua et al., 2020
8	Neophytadiene	C20H38	278.52	17.516	2.48	Diterpenes	anti-inflammatory, anti-microbial, antioxidant	Akter et al., 2024
9	Neophytadiene	C20H38	278.52	17.705	3.69	Diterpenes	anti-inflammatory, anti-microbial, antioxidant	Akter et al., 2024
10	Hexadecanoic acid, methyl ester	C17H34O2	270.45	18.163	20.2	Fatty acid ester	Antioxidant, anticancer, antidiabetic, nephroprotective, anti-inflammatory, and antibacterial	Akter et al., 2024
11	n-Hexadecanoic acid	C16H32O2	256.42	18.538	2.17	Fatty acid	Anti-inflammatory antimicrobial, antioxidant, anticancer Antitumor & Hypocholesterolemic	Akter et al., 2024
12	9,12-Octadecadienoic acid (Z,Z)-, methyl ester	C19H34O2	294.47	19.781	3.43	Fatty acid ester	Antioxidant, antimicrobial, and anti-inflammatory	Akter et al., 2024
13	9-Octadecenoic acid, methyl ester, (E)-	C19H36O2	296.49	19.837	14.9	Fatty acid ester	Antimicrobial, Antifungal, Antioxidant	Akkoyunlu et al., 2022
14	9-Octadecenoic acid (Z)-, methyl ester	C19H36O2	296.49	19.905	0.68	Fatty acid ester	Antimicrobial, Antifungal, Antioxidant	Akkoyunlu et al., 2022
15	Phytol	C20H40O	296.53	19.939	0.84	Diterpene alcohol	Antioxidant, antidiabetic, anticancer, anti-inflammatory, antitumor, chemoprotective, antimicrobial, antiprotozoal, histamine release inhibitor, and antimicrobial	Akter et al., 2024
16	Methyl stearate	C19H38O2	298.5	20.078	3.19	Fatty acid methyl ester	Anti-inflammatory, antidiarrheal, cytotoxic,	Akter et al., 2024

							antiproliferative, and antioxidant	
17	Hexatriacontane	C36H74	506.97	24.718	1.32	Hydrocarbon	Antibacterial, Antiviral, Antioxidant	Aadesariya et al., 2018
18	Tetracosane	C24H50	338.65	26.116	0.56	Hydrocarbon	Antimicrobial, Antifungal, Antioxidant	Akkoyunlu et al., 2022
19	Tetracontane	C40H82	563.08	27.425	0.83	Hydrocarbon	Antifungal	Pavirhra et al., 2020
20	Octacosanol	C28H58O	410.76	27.48	0.87	Fatty acid alcohol	anticancer activity, hypocholesterolemic agent, anticoagulant activity	Umoh et al., 2025
21	.beta.-Sitosterol acetate	C31H52O2	456.74	27.514	1.26	Triterpenoid	Antimicrobial	Nweze et al., 2019
22	alpha.-Tocopherol-.beta.-D-mannoside	C35H60O7	592.85	27.665	0.61	Vitamin E	Antidiabetic, Antioxidant	Chike-Ekwughe et al., 2023
23	Phytyl stearate	C38H74O2	562.99	27.769	0.98	Fatty acid ester	Not found	
24	16-Hentriacontanone	C31H62O	450.82	28.63	11.87	dialkyl ketone	Antimicrobial	Shanker et al., 2005
25	gamma-sitosterol	C29H50O	414.71	29.032	5.42	Phytosterol	Antidiabetic (Increase insulin secretion and inhibit glucogenesis)	Akter et al., 2024

4.3. Total Phenolic Content

A standard calibration curve was constructed using gallic acid as the reference phenolic compound (fig. 2A). The absorbance values obtained from the plant extract were then compared against this standard curve to determine the phenolic concentration. The TPC of the *A. ampeloprasum* extract was found to be 15.45 ± 0.51 mg gallic acid equivalents (GAE) per gram of extract (fig. D). These results indicate a moderate presence of phenolic compounds, which are known to contribute to the antioxidant properties of plant-based extracts.

4.4. Total Flavonoid Content

Quantification of TFC was performed using the aluminum chloride colorimetric method. A standard calibration curve was generated using quercetin as the reference flavonoid compound, as shown in fig. 2 B. The absorbance values of the plant extract were measured and compared to this standard curve to estimate the flavonoid concentration. The TFC of the *A. ampeloprasum* extract was determined to be 21.71 ± 0.51 mg quercetin equivalents (QE) per gram of extract, as illustrated in fig. 2 D. The relatively high flavonoid content suggests the potential of *A. ampeloprasum* as a natural source of antioxidant compounds.

4.5. DPPH Assay

The antioxidant potential of the sample was assessed using the DPPH (2,2-diphenyl-1-picrylhydrazyl) radical scavenging assay across a concentration range of 10 to 100 µg/mL. The percentage radical scavenging activity (%RSA) demonstrated a clear concentration-dependent increase, rising from 50.74% at 10 µg/mL to 93.70% at 100 µg/mL, indicating strong antioxidant potential. The regression equation obtained from the plotted data was y = 0.4466x + 49.334 with an R^2 value of 0.9829. This linearity confirms the reliability of the experimental results (Figure 3C). To quantify the effectiveness of the sample, the IC_{50} value (the concentration required to scavenge 50% of DPPH radicals) was calculated using the following interpolation formula:

$$IC50 = C1+(\%RSA2-\%RSA150-\%RSA1) \times (C2-C1)$$

Where:

C_1 = 10 µg/mL (concentration at $\%RSA_1$ = 50.74)

C_2 = 20 µg/mL (concentration at $\%RSA_2$ = 60.19)

This low IC_{50} value of 9.22 µg/mL indicates that the sample possesses potent free radical scavenging ability, consistent with previously reported results (Kumar et al., 2014).

4.6. Antibacterial studies

Well diffusion assay

The antibacterial efficacy of *A. ampeloprasum* leaf extracts was assessed using five different concentrations (1000 µL/mL, 500 µL/mL, 250 µL/mL, 125 µL/mL, and 50 µL/mL) through the well diffusion assay. The study targeted four bacterial strains, including two Gram-positive (*Bacillus subtilis* and *Staphylococcus aureus*) and two Gram-negative bacteria (*Escherichia coli* and *Pseudomonas aeruginosa*). The zones of inhibition (ZOI) were obtained for each bacterial strain at the various extract concentrations table 2. The concentration-dependent antibacterial activity and the differential susceptibility of the bacterial strains to the extracts are given in fig, 3. Graphical representation of ZOI obtained with *A. ampeloprasum* extracts with positive control (ciprofloxacin) against four bacterial strains are presented in fig, 4.

The highest zone of inhibition (ZOI) was observed against *B. subtilis* across all tested concentrations. The recorded ZOI values were as follows: 10 ± 0.34 mm at 1000 µL/mL, 8 ± 0.44 mm at 500 µL/mL, 7 ± 0.37 mm at 250 µL/mL, 7 ± 0.43 mm at 125 µL/mL, and 7 ± 0.15 mm at 50 µL/mL. In contrast, *S. aureus* exhibited minimal inhibition, with a ZOI of 6 ± 0.64 mm observed only at the highest concentration of 1000 µL/well. *P. aeruginosa* showed consistent ZOI values of 6 ± 0.33 mm across the concentrations of 1000, 500, and 250 µL/mL. Similarly, *E. coli* demonstrated its maximum ZOI of 7 ± 0.05 mm at 1000 µL/mL, with similar inhibition levels of 6 ± 0.04 mm at both 500 and 250 µL/mL.

Table 2. Zone of Inhibition (mm) obtained against four different bacterial strains

Amount (µg/well)	*S. aureus*	*P. aeruginosa*	*E. coli*	*B. subtilis*
PC	30	27.33	28.66	28.66
0	0	0	0	0
50	0	0	0	5.5 ±0.66
125	6 ± 0.56	6 ± 0.064	5 ± 0.16	6.2 ± 0.15
250	6.33± 0.64	7 ± 0.77	5 ± 0.47	6.7 ±0.64
500	7.33 ± 0.399	7.33 ± 0.21	5.55 ± 0.33	7. 0 ± 0.11
1000	7.33 ± 0.322	8 ± 0.54	7.44 ± 0.26	10 ± 0.55

4.7. In silico Docking Studies

The GC–MS analysis revealed that *A. ampeloprasum* leaf methanolic extracts contained 21 different bioactive compounds. However, 3D structure of 9-Octadecenoic acid methyl ester (E)-, 9-Octadecenoic acid (Z)-methyl ester, Methyl sterate, Hexatriacontane, Tetracosane, Tetracontane, Octacosanol, beta-sitosterol are not avaliabe on Pubchem (Kim et al., 2016). All the available compounds with their Compound ID, Canonical smiles and 3D structure represents in table 3. These identified compounds were subjected to molecular docking studies against DNA Gyrase by using Autodock vina (Morris et al., 2009). Out of twenty-one GC-MS identified compounds, only four compounds namely 2-Pentadecanone, 6, 10, 14-trimethyl-, gamma-sitosterol, Neophytadiene and Phytol shows binding interaction with DNA gyrase. The compound gamma-sitosterol formed highest binding energy i.e., -7.1 kcal/mol out of selected compounds with one conventional H bond against DNA gyrase at ASP 73. Binding interactions of all interacted compounds of *A. ampeloprasum* with interacting amino acid were analysed using Discovery Studio Vizualizer (Design et al., 2014) (fig. 5a & 5b, table 4). The different bonding interactions of ligand and protein residues are hydrogen, hydrophobic (alkyl), hydrophobic (pi-alkyl), pi-lone pair (table 3).

Table 4. Docking of DNA gyrase with compounds identified through GC-MS analysis

Compound name	Type of H Bond	Binding Energy with alpha amylase	Number of H bonds involved in bonding	Amino acid involved in H bond
Ciprofloxin	Conventional H-Bond, Alkyl, Pi-Alkyl, Pi-Anion	-7.1	2	Asn 46, Thr 165
2-Pentadecanone, 6,10,14-trimethyl-	Alkyl Bond	-4.9		
Gamma-sitosterol	Conventional H-Bond, Alkyl Bond	-7.1	1	Asp 73
Neophytadiene	Alkyl	-5.6		
Phytol	Conventional H-Bond, Alkyl Bond	-5.1	1	Val 167

5. Molecular Dynamic Simulation

5.1. Root Mean Square Deviation (RMSD) Analysis

The Root Mean Square Deviation (RMSD) is a crucial parameter for quantifying the extent of conformational changes in proteins during molecular dynamics (MD) simulations. In this study, the RMSD of the Cα atoms from their initial structures was calculated to evaluate the stability of the protein-ligand complexes. The time-dependent RMSD of the backbone atoms of DNA gyrase in both free and ligand-bound states was observed to range between 0.2nm to 0.25nm, the plateau is remaining stabilize from 0 to 100 ns throughout the simulation. The range of ciprofloxacin (standard antibacterial drug) and gamma-sitosterol are overlapping during whole simulation. This indicates a high degree of stability with DNA gyrase in its ligand-bound conformations. It has been observed that the RMSD values for all systems remained below 0.3 nm throughout the simulation period (fig. 6A) with minimal deviation of the enzyme from its starting conformation indicates the stability of complex. Furthermore, the binding of phytomolecules did not induce significant conformational changes in the protein backbone. This affirms the structural stability of DNA gyrase protein in the presence of ligands.

5.2. Flexibility and Dynamics Analysis Using Root Mean Square Fluctuation (RMSF)

The flexibility and dynamics of the system were assessed through RMSF analysis. The majority of the enzyme residues exhibited RMSF values ranging from 0.2 to 0.5 nm (fig.6 B). This value indicates minimal fluctuations. This observation suggests that the positional stability of the amino acid residues remains largely unaffected by the binding of the phytochemical to the active site of enzyme DNA gyrase. Consequently, it can be concluded that the ligand-protein interaction does not significantly alter the overall dynamics of the protein.

5.3. Radius of Gyration Analysis (Rg)

The radius of gyration (Rg) serves as a measure of protein compactness, with lower Rg values indicating greater stability. Since ligand binding can potentially induce protein unfolding, the variation in Rg was analyzed throughout the simulation for all cases. For the unbound state of DNA gyrase (control), the Rg values were centered around ~1.6 nm. Similarly, Rg values ranging from ~1.58 to 1.62 nm were observed with ligand bound state phytomolecules i.e., ciprofloxacin, gama-sitosterol and phytol (fig.6C). These results indicate that the binding of the phytomolecules does not affect the structural integrity or compactness of DNA gyrase.

5.4 Solvent Accessible Surface Area (SASA) Analysis

Hydrophobic interactions between non-polar amino acids play an important role in stabilizing globular proteins by shielding these residues within hydrophobic cores from the aqueous environment. The solvent-accessible surface area (SASA) provides a theoretical measure of changes in protein accessibility to solvent, reflecting the contribution of free energy of solvation for each atom in the system, including water, and the polar and non-polar amino acids of the protein. In the case of unbound DNA gyrase (control), SASA profile peaked at approximately ~95-98 nm². Upon binding with ligands, the SASA values shifted to a range of ~95–105nm² (fig.6 D). Since the observed SASA values show minimal deviation compared to the control, it can be inferred that the binding of these compounds does not disrupt protein folding or alter the structural integrity of protein.

5.5. Hydrogen Bond Analysis

The hydrogen bond interactions between DNA gyrase and the bioactive metabolites were evaluated using the hydrogen bond module of GROMACS. The distribution of hydrogen bonds was monitored throughout the 100 ns simulation, with the maximum hydrogen bond distances ranging from 0.25 to 0.35 nm. The hydrogen bond distribution graph (fig.6 F) indicated that hydrogen bond formation initiated at a distance of 0.25 nm between the hydrogen bond donor and acceptor, with the maximum distribution observed at a distance of 0.30 nm. These findings highlight the stability and optimal geometry of hydrogen bond interactions (fig.6 E) in the ligand-receptor complex. The average values of different parameters of molecular dynamics simulation are given in table 5.

Table 5: The average values of different parameters of molecular dynamics simulation

Sr. no.		Control (DNA gyrase)	Ciprofloxacin	Gamma-sitosterol	Phytol
1	Backbone RMSD	0.128 ± 0.0313	0.126±0.036	0.189±0.021	0.972±0.030
2	Complex RMSD	-	0.620±0.0661	0.273±0.035	0.340±0.030
3	Ligand RMSD	-	0.079±0.018	0.082±0.017	0.070±0.015
4	Radius of Gyration	1.586±0.180	1.592±0.177	1.581±0.173	1.584±0.172
5	SASA	133.438±4.394	134.850±3.887	133.236±2.737	135.263±3.025
6	RMSF	0.125±0.101	0.128±0.098	0.119±0.072	0.125±0.092

5. Binding Free Energy Analysis

The binding free energy (ΔGbind) of the ligand-protein complexes was calculated using Molecular Mechanics Poisson-Boltzmann Surface Area (MMPBSA) analysis. This provides insights into the binding potential of the ligands. The MMPBSA results confirmed that all tested molecules viz. ciprofloxacin, gamma-sitosterol and phytol are successfully bind to the active site of target protein to form stable complexes. The variation in ΔGbind values was primarily influenced by the van der waals interaction component (ΔEvdw) and the polar solvation free energy component (ΔGpsolv), which played significant roles in lowering the binding free energy. Additional energy components, including electrostatic energy (ΔEEL), polar solvation energy (ΔGpsolv), and nonpolar solvation energy (ΔGnpsolv), also contributed to the overall binding free energy of the enzyme-ligand complexes. The detailed MMPBSA results for all ligands are given in fig. 7 and table 6.

Table 6: Free energy depiction of protein ligand-complex (KJ/mol) through MMPBSA analysis

S.N	Compound	$\Delta E_{VDWAALS}$	ΔE_{EL}	ΔE_{PB}	ΔE_{NPOLAR}	ΔG_{GAS}	ΔG_{SOLV}	ΔTotal
1	Ciprofloxacin	-31.39±3.32	-24.00±2.3	33.21±1.9	-2.99±0.06	-55.40±3.5	30.21±2.09	-25.128±2.61
2	Gamma-sitosterol	-37.12±3.16	-13.74±2.461	30.21±2.67	-3.73±0.071	-50.86±2.88	26.48±2.64	-24.38±1.11
3	Phytol	-29.33±1.84	-26.875±1.60	30.912±4.15	-3.347±0.12	-56.20±2.052	27.56±1.66	-28.64±3.05

6. Principal Component Analysis (PCA)

Principal component analysis was utilized to investigate the conformational dynamics of the protein upon binding with ciprofloxacin, gamma-sitosterol, and phytol, highlighting the dominant collective motions during molecular dynamics (MD) simulations. The PCA scatter plots in figures 8 A, 8 B, and 8 C represent the distribution of conformations along the principal components PC1, PC2, and PC3 for each complex. The color gradient from red to blue reflects decreasing rigidity and increasing atomic mobility, with red indicating the least fluctuation, white intermediate, and blue the most dynamic regions. For the ciprofloxacin-bound complex, PC1 accounted for 18.01% of the total motion, followed by PC2 and PC3, each contributing 8.39%. In the gamma-sitosterol-bound system, PC1 exhibited higher motion at 23.91%, with PC2 and PC3 contributing 8.62% and 6.8%, respectively. The phytol-bound protein showed the most dominant motion in PC1 at 47.37%, while PC2 and PC3 contributed 9% and 5.38%, respectively. The eigenvalue graphs for all complexes demonstrated a steep decline in variance after the first few eigenvectors. This confirms that the majority of the motion was captured by the top five principal components. This indicates that ciprofloxacin and gamma-sitosterol induce moderate dynamic fluctuations, whereas phytol binding results in pronounced conformational changes along PC1, indicating more significant structural

rearrangements. In contrast, the minimal variability in PC3 across all systems reflects a relatively stable and compact protein-ligand complex in that principal component space.

Discussion

The growing concern of antimicrobial resistance has renewed interest in natural bioresources as alternative or complementary therapies. Within this context, species of the *Allium* genus have consistently demonstrated significant bioactive potential, particularly due to their rich reservoir of secondary metabolites. Our findings align with numerous prior reports, which highlight the strong antibacterial and antioxidant efficacy of *Allium ampeloprasum* extracts. Specifically, the methanol extract showed notable zones of inhibition against both gram-positive and gram-negative bacteria, including *Bacillus subtilis*, *Escherichia coli*, and *Pseudomonas aeruginosa*. These outcomes validate the findings of Dziri et al. (2012) and Bareemizadeh et al. (2014), who reported similar efficacy of *Allium* extracts. This implies that differences in bacterial susceptibility may result from variations in extraction solvents, phytochemical composition, or bacterial strain types.

Interestingly, the inconsistency in antibacterial response across studies, such as the lack of effect on *P. aeruginosa* and *B. subtilis* reported by Añides et al. (2021) highlights the complex nature of plant-based bioactivity. Nevertheless, our findings support that *A. ampeloprasum* extract possesses clear antibacterial effects, particularly against *B. subtilis* (10 ± 0.34 mm), and also retains moderate activity against *E. coli* and *P. aeruginosa*. This supports the hypothesis that phenolic and flavonoid compounds are instrumental in disrupting microbial integrity and function.

Beyond antimicrobial properties, *A. ampeloprasum* displayed exceptional antioxidant potential. The extract's low IC_{50} value (0.193 µg/mL) and high DPPH radical scavenging efficiency suggest strong electron-donating capacity. These effects are consistent with findings by Caputo et al. (2022) who reported up to 87.3% DPPH inhibition in methanolic extracts. The total phenolic (TPC: 11.45 ± 0.51 mg GAE/g) and flavonoid content (TFC: 21.71 ± 0.51 mg QE/g) further confirm that antioxidant and antimicrobial activities are largely driven by these secondary metabolites, which function by scavenging reactive oxygen species (ROS) and potentially disrupting bacterial membranes and metabolic pathways. Complementing our experimental results, in silico docking and molecular dynamics simulations offered deeper insight into the mechanism of action at the molecular level. Gamma-sitosterol, a major phytosterol present in *Allium* species, displayed strong affinity for DNA gyrase, the same enzymatic target as ciprofloxacin. With a binding energy of −7.1 kcal/mol and a hydrogen bond formed at ASP 73, gamma-sitosterol mimicked ciprofloxacin's interaction profile. Moreover, MD simulation parameters—including RMSD, RMSF, SASA, and radius of gyration—validated the structural stability of the gamma-sitosterol–enzyme complex, indicating its potential to inhibit bacterial DNA replication.

However, a crucial discrepancy lies in the pharmacokinetic profile of these compounds. Ciprofloxacin boasts high systemic bioavailability, rapid absorption, and renal excretion, making it a potent and predictable therapeutic agent. Gamma-sitosterol, in contrast is hindered by poor aqueous solubility and limited intestinal absorption though its lipophilic nature enables effective interactions at membrane-rich sites. While its clinical application may currently be limited, gamma-sitosterol's binding behavior presents an exciting opportunity for chemical optimization and drug development aimed at enhancing solubility and systemic availability.

Altogether, this integrated approach combining traditional microbiological assays, phytochemical profiling, and computational modelling demonstrates the therapeutic promise of *A. ampeloprasum* as a natural reservoir of potent antimicrobial and antioxidant agents. The strong correlation between in vitro activity and in silico predictions not only validates the biological relevance of gamma-sitosterol but also paves the way for novel phytochemical-based drug discovery targeting bacterial DNA replication pathways. Given the growing resistance to existing antibiotics, such compounds offer a valuable starting point for the development of next-generation therapeutics derived from plant-based sources.

Conclusion

This study establishes *Allium ampeloprasum* leaf extract as a potent natural source of antioxidant and antibacterial agents. Phytochemical analysis revealed notable levels of phenolics (TPC: 11.45 ± 0.51 mg GAE/g) and high flavonoids (TFC: 21.71 ± 0.51 mg QE/g), supporting its strong antioxidant activity, evidenced by a concentration-dependent DPPH scavenging effect (50.74%–93.70%) and a low IC_{50} value of 9.22 µg/mL (R^2 = 0.9829). Antibacterial evaluation showed selective activity, with *Bacillus subtilis* being most sensitive (10 ± 0.34 mm), followed by *E. coli* and *P. aeruginosa*, while *S. aureus* showed minimal response. Molecular docking and MD simulation confirmed stable interactions of key compounds like gamma-sitosterol and phytol with bacterial targets, particularly DNA gyrase, with binding affinities comparable to ciprofloxacin. These findings indicate promising therapeutic potential and justify further in

vitro and in vivo investigations of unreported constituents such as 2-Pentanol acetate and Phytyl stearate. Despite its medicinal value, *A. ampeloprasum* remains underutilized in India. It is currently cultivated in parts of Uttarakhand, Manipur, and Kashmir. Given its adaptability and bioactive richness, it should be promoted for cultivation in new regions to enhance dietary value, develop functional foods, and support phytopharmaceutical innovation. This approach may also help identify superior genotypes for medicinal plant-based agriculture and rural income generation.

Declarations

9. Acknowledgement

The authors gratefully acknowledge the Department of Botany and Department of Microbiology, Chaudhary Charan Singh University, Meerut, for providing essential research facilities. Special thanks to Dr. K.M. Rai, ICAR-NBPGR Regional Station, Bhowali (Nainital, Uttarakhand), for supplying *Allium* saplings. The study was financially supported by the Council of Scientific and Industrial Research (CSIR), New Delhi.

References

1. Aadesariya, M. K., Ram, V. R., & Dave, P. N. (2018). Phytochemical analysis of leaves extract of *Abutilon pannosum* in n-butanol for its bioactive components through gas chromatography-mass spectrometry (GC-MS). *Phytochemical Analysis, 8*(9).
2. Aiyegroro OA, Okoh AI. Preliminary phytochemical screening and in vitro antioxidant activities of aqueous extract of Helichrysum longifolium DC. BMC compl. And. Alt. Med., (2010), 10:21.
3. Akkoyunlu, A., & Dulger, G. (2022). Chemical composition and in vitro antimicrobial, antioxidant, and antiproliferative studies of the *Lamium galeobdolon* L. (L.) essential oil. *Russian Journal of Bioorganic Chemistry, 48*(6), 1240–1246.
4. Akter, R., Maknun Fariha, L., Halder, S., Sharmin, S., Sabet Taki, E., Kabir Lihu, I., ... & Sharmin, S. (2024). GC-MS employed phytochemical characterization and anticancer, antidiabetic, and antioxidant activity screening of *Lagerstroemia thorelli*. *Chemistry & Biodiversity, 21*(12), e202400999.
5. Al-Dabbas, M. M., Saleh, N. A., & Al-Ismail, K. (2010). Antioxidant and antimicrobial activity of leek (*Allium ampeloprasum* L.) extract in preserving meat. *Journal of Food Protection, 73*(3), 497–502.
6. Aliye, M., Dekebo, A., Tesso, H., Abdo, T., Eswaramoorthy, R., & Melaku, Y. (2021). Molecular docking analysis and evaluation of the antibacterial and antioxidant activities of the constituents of *Ocimum cufodontii*. *Scientific Reports, 11*(1), 10101.
7. Amos-Tautua, B. M., Alayande, K. A., Ajileye, O., Fadare, O. A., & Songca, A. O. S. P. (2020). Effect of the leaf extracts of *Funtumia africana* (Benth.) Stapf. against selected pathogens. *Journal of Medicinal Plants Studies, 8*(4), 125–129.
8. Añides, J. A., Dapar, M. L. G., Aranas, A. T., Mindo, R. A. R., Manting, M. M. E., Torres, M. A. J., & Demayo, C. G. (2019). Phytochemical, antioxidant and antimicrobial properties of the white variety of 'Sibujing' (*Allium ampeloprasum*). *Pharmacophore, 10*(1), 1–12.
9. Bareemizadeh, F., Ghasempour, H., Maassoumi, S. M., Karimi, N., Taran, M., & Ghasempour, M. (2014). In vitro antimicrobial activity of *Allium ampeloprasum* L. var. *atroviolaceum* Regel.
10. Bauer, A. W., Kirby, W. M. M., Sherris, J. C., & Turck, M. (1966). Antibiotic susceptibility testing by a standardized single disk method. *American Journal of Clinical Pathology, 45*(4), 493–496.
11. Benzie, I. F. F., & Strain, J. J. (2011). Analysis of bioactive components in garlic. *Journal of Agricultural and Food Chemistry, 59*(10), 5371–5378.
12. Berendsen, H. J., Postma, J. V., Van Gunsteren, W. F., DiNola, A. R. H. J., & Haak, J. R. (1984). Molecular dynamics with coupling to an external bath. *The Journal of chemical physics*, *81*(8), 3684-3690.
13. Borlinghaus, J., Albrecht, F., Gruhlke, M. C., Nwachukwu, I. D., & Slusarenko, A. J. (2014). Allicin: Chemistry and biological properties. *Molecules, 19*(8), 12591–12618.
14. Brand-Williams, W., Cuvelier, M. E., & Berset, C. L. W. T. (1995). Use of a free radical method to evaluate antioxidant activity. *LWT - Food Science and Technology, 28*(1), 25–30.
15. Campoli-Richards, D. M., Monk, J. P., Price, A., Benfield, P., Todd, P. A., & Ward, A. (1988). Ciprofloxacin: a review of its antibacterial activity, pharmacokinetic properties and therapeutic use. *Drugs*, *35*, 373-447.

16. Caputo, L., Amato, G., Fratianni, F., Coppola, R., Candido, V., De Feo, V., & Nazzaro, F. (2020). Chemical characterization and antibiofilm activities of bulbs and leaves of two aglione (*Allium ampeloprasum* var. *holmense* Asch. et Graebn.) landraces grown in Southern Italy. *Molecules, 25*(23), 5486.
17. Chike-Ekwughe, A., Adegboyega, A. E., Johnson, T. O., Adebayo, A. H., & Ogunlana, O. O. (2023). In vitro and in-silico inhibitory validation of *Tapinanthus cordifolius* leaf extract on alpha-amylase in the management of type 2 diabetes. *Informatics in Medicine Unlocked, 36*, 101148.
18. Teotia, D., Agrawal, A., Goyal, H., Jain, P., Singh, V., Verma, Y., ... & Malik, V. (2024). Pharmacophylogeny of genus *Allium* L. *Journal of King Saud University-Science*, *36*(8), 103330.
19. Design, L. I. G. A. N. D. (2014). Pharmacophore and ligand-based design with Biovia Discovery Studio *BIOVIA. California.*
20. Devi, A., Rakshit, K., & Sarania, B. (2014). Ethnobotanical notes on *Allium* species of Arunachal Pradesh, India. *Indian Journal of Traditional Knowledge, 13*(3), 606–612.
21. Dey, P., & Khaled, K. L. (2015). An extensive review on Allium ampeloprasum: A magical herb. *International Journal of Science and Research, 4*(7), 371–377.
22. Dey, P., & Khaled, K. L. (2015). An extensive review on *Allium ampeloprasum*: A magical herb. *International Journal of Science and Research, 4*(7), 371–377.
23. Guhabakshi, D. N., Sensarma, P., & Pal, D. C. (1999). *A lexicon of medicinal plants in India* (Vol. 1). Naya Prokash.
24. Hooper, D. C., & Jacoby, G. A. (2016). Mechanisms of drug resistance: quinolone resistance. *Annals of the New York Academy of Sciences*, 1354(1), 12–31. https://doi.org/10.1111/nyas.12954
25. Jain, P., Kumar, V., Teotia, D., Goyal, H., Agrawal, A., & Malik, V. (2024). Phytochemical composition of *Sida rhombifolia* ssp. *retusa* (L.) Bross.: A comprehensive GC/MS analysis. *Journal of Xi'an Shiyou University, Natural Sciences Edition, 3*.
26. Jang, J. H., Moon, J. H., & Yoon, H. M. (2018). Identification and quantification of antioxidant compounds in onions. *Food Science and Biotechnology, 27*(3), 623–630.
27. Kaneria, M., Kanani, B., & Chanda, S. (2012). Assessment of effect of hydroalcoholic and decoction methods on extraction of antioxidants from selected Indian medicinal plants. *Asian Pacific Journal of Tropical Biomedicine, 2*(3), 195–202.
28. Khandelwal, K. R. (2008). *Practical Pharmacognosy* (19th ed., pp. 149–156, 157–159). Nirali Prakashan.
29. Kim, S., Lee, J. Y., & Park, J. Y. (2018). Antioxidant activities of phenolic and flavonoid compounds in Allium species. *Food Chemistry, 245*, 63–72.
30. Kumar, S., Sandhir, R., & Ojha, S. (2014). Evaluation of antioxidant activity and total phenol in different varieties of Lantana camara leaves. *BMC research notes*, *7*, 1-9.
31. Liguori, I., Russo, G., Curcio, F., Bulli, G., Aran, L., Della-Morte, D., ... & Testa, G. (2018). Oxidative stress, aging, and diseases. *Clinical Interventions in Aging, 13*, 757–772.
32. Morris, G. M., Huey, R., Lindstrom, W., Sanner, M. F., Belew, R. K., Goodsell, D. S., & Olson, A. J. (2009). AutoDock4 and AutoDockTools4: Automated docking with selective receptor flexibility. *Journal of computational chemistry*, *30*(16), 2785-2791.
33. Muhsin, J., Ufaq, T., Tahir, H., & Saadia, A. (2015). Bacterial biofilm: Its composition, formation and role in human infection. *Journal of Microbiology and Biotechnology, 4*, 1–14.
34. Najeebullah, S., Shinwari, Z. K., Jan, S. A., Khan, I., & Ali, M. (2021). Ethnomedicinal and phytochemical properties of genus *Allium*: A review of recent advances. *Pakistan Journal of Botany, 53*(1), 135–144.
35. Nweze, C., Ibrahim, H., & Ndukwe, G. I. (2019). Beta-sitosterol with antimicrobial property from the stem bark of pomegranate (*Punica granatum* Linn). *Journal of Applied Sciences and Environmental Management, 23*(6), 1045–1049.
36. Pavirhra, R., & Lalitha, S. (2020). Tetradecane producing biocontrol agent, *Trichoderma* spp. against *Fusarium oxysporum* in tomato (*Solanum lycopersicum* L.). *International Journal of Agricultural Technology*, 16(6), 1475-1492.
37. Putnik, P., Gabrić, D., Roohinejad, S., Barba, F. J., Granato, D., Mallikarjunan, K., ... & Kovačević, D. B. (2019). An overview of organosulfur compounds from *Allium* spp.: From processing and preservation to evaluation of their bioavailability, antimicrobial, and anti-inflammatory properties. *Food Chemistry, 276*, 680–691.
38. Rababah, T. M., Al-Mahasneh, M. A., Ereifej, K., Alhamad, M. N., Al-Karaki, G. N., Yang, W., & Al-U'datt, M. (2015). Effect of plant extracts on the shelf life of fresh poultry meat. *Poultry Science, 94*(1), 6–13.
39. Reddy, G. S., Srinivasulu, K., Mahendran, B., & Reddy, R. S. (2018). Biochemical characterization of anti-microbial activity and purification of glycolipids produced by dodecanoic acid-undecyl ester. *Research Journal of Pharmacy and Technology, 11*(9),

4066–4073.

40. Reece, R. J., & Maxwell, A. (1991). DNA gyrase: structure and function. *Critical reviews in biochemistry and molecular biology*, *26*(3-4), 335-375.
41. Reuter, S., Gupta, S. C., Chaturvedi, M. M., & Aggarwal, B. B. (2010). Oxidative stress, inflammation, and cancer: How are they linked? *Free Radical Biology and Medicine, 49*(11), 1603–1616.
42. Shanker, K. S., Kanjilal, S., Rao, B. V. S. K., Kishore, K. H., Misra, S., & Prasad, R. B. N. (2007). Isolation and antimicrobial evaluation of isomeric hydroxy ketones in leaf cuticular waxes of *Annona squamosa*. *Phytochemical Analysis, 18*(1), 7–12.
43. Sloggett C, Goonasekera N, Afgan E (2013) BioBlend: automating pipeline analyses within Galaxy and CloudMan. Bioinformatics 29(13):1685–1686. https://doi.org/10.1093/bioinformatics/btt199
44. Tavakkoli, A., Oboudi, B., & Tavakkoli, A. (2015). Antibacterial effects of water extracts of various broadleaf wild leeks (*Allium ampeloprasum*). *Journal of Pharmacy and Pharmacology, 3*(9), 438–442.
45. Ukwubile, C. A., Ahmed, A., Katsayal, U. A., Ya'u, J., & Mejida, S. (2019). GC–MS analysis of bioactive compounds from *Melastomastrum capitatum* (Vahl) Fern. leaf methanol extract: An anticancer plant. *Scientific African, 3*, e00059.
46. Umoh, R. A., Asanga, E. E., Thomas, P. S., Umoh, U. F., Johnny, I. I., Essiett, U. A., & Joseph, A. (2025). Isolation of a lauryl alcohol (1-dodecanol) from the antioxidant bioactive fractions of *Justicia insularis* (Acanthaceae) leaves. *Natural Product Communications, 20*(1), 1934578X241297510.
47. Vanommeslaeghe, K., Hatcher, E., Acharya, C., Kundu, S., Zhong, S., Shim, J., ... & Mackerell Jr, A. D. (2010). CHARMM general force field: A force field for drug-like molecules compatible with the CHARMM all-atom additive biological force fields. *Journal of computational chemistry*, *31*(4), 671-690.

Figures

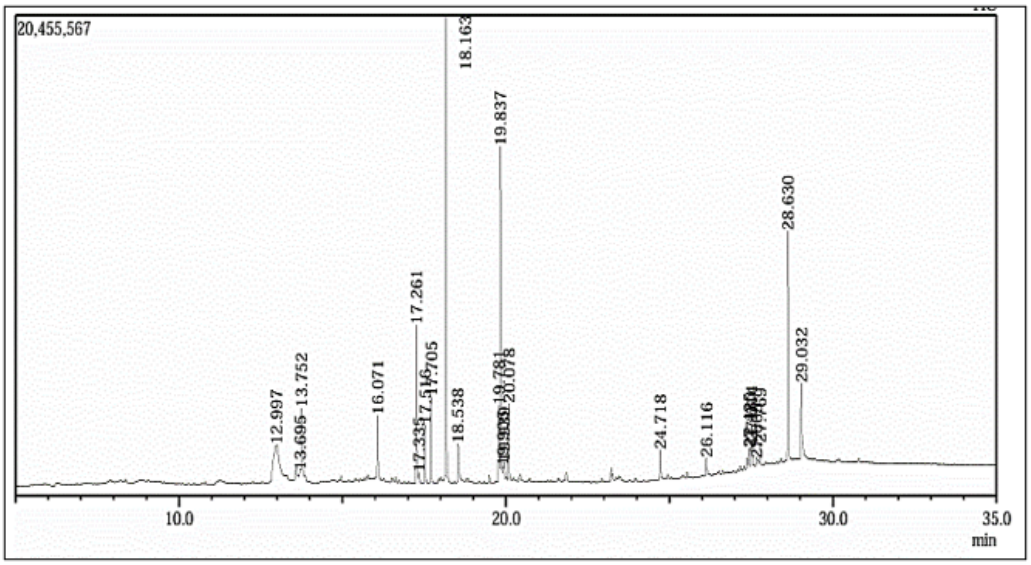

Figure 1

GC-MS Chromatogram of methanolic extract of the leaves of *A. ampeloprasum*

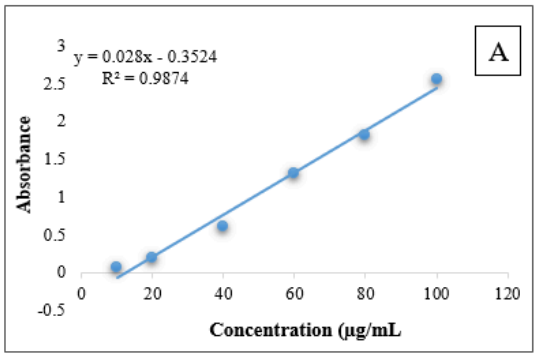

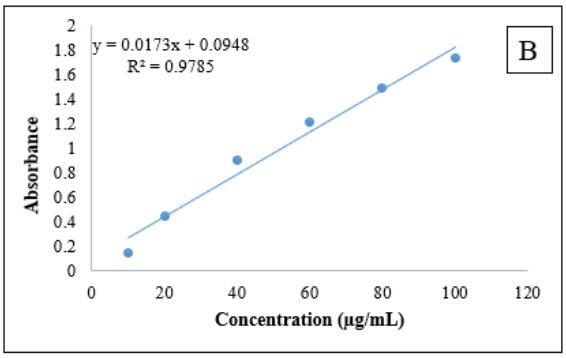

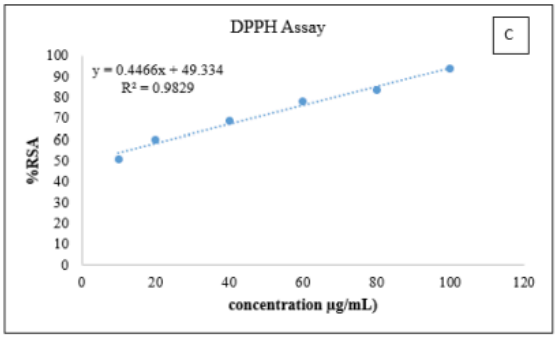

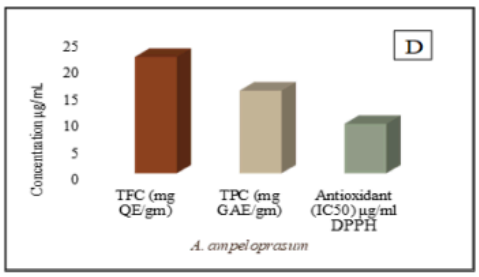

Figure 2

A) Standard curve TPC, B) Standard curve TFC, C) Standard curve DPPH assay D) Graphical representation of Total Flavonoid Content (TFC), Total Phenolic Content (TPC) and IC_{50} value of *A. ampeloprasum* leaf extract

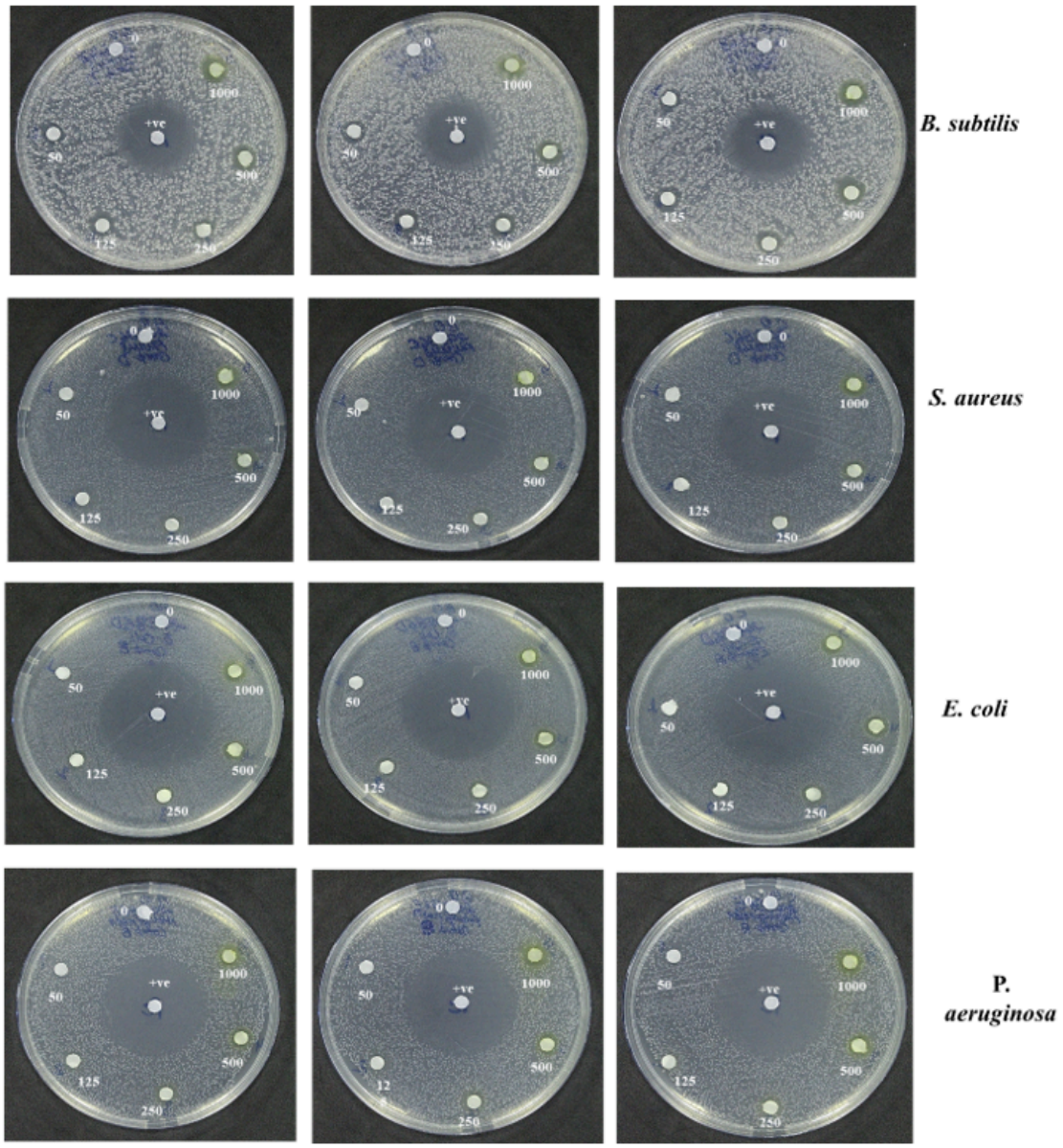

Figure 3

ZOI obtained with *A. ampeloprasum* leaf extract against four different bacterial strains

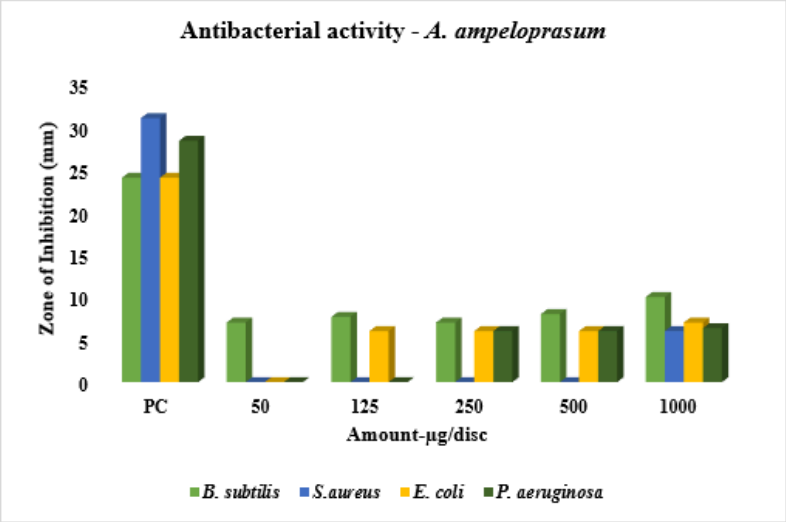

Figure 4

Graphical representation of ZOI obtained with *A. ampeloprasum* extracts and positive control against four bacterial strains

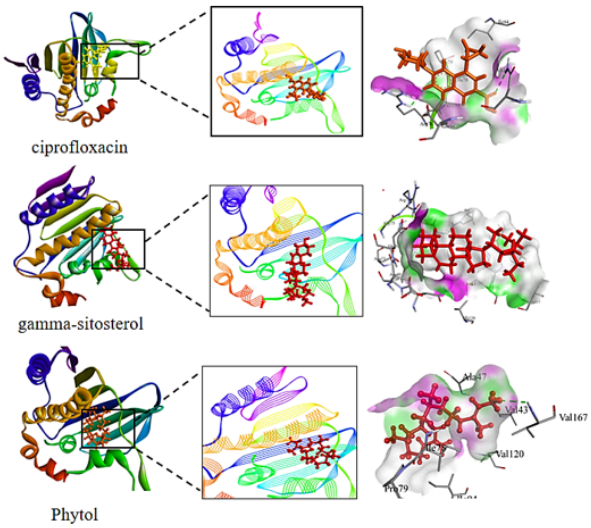

Fig 5a

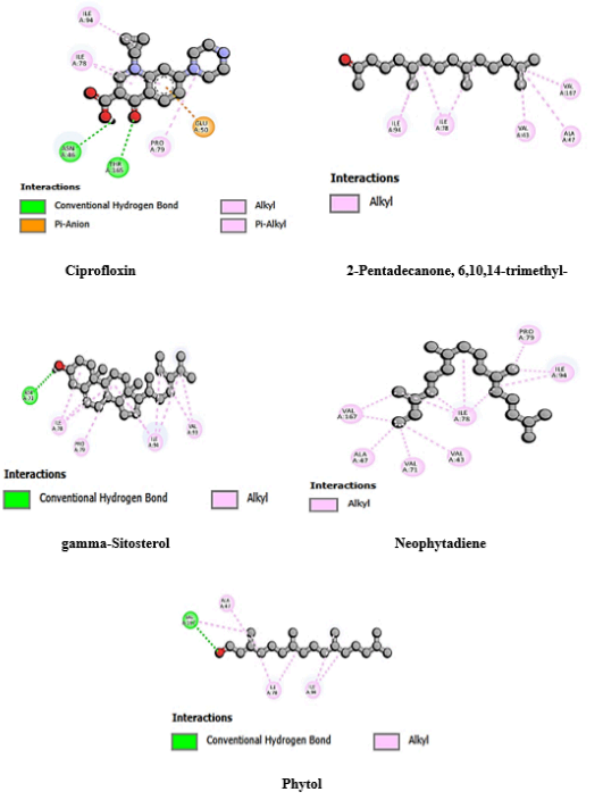

Fig 5b

Figure 5

a. Docking interaction compounds identified through GC-MS analysis against DNA gyrase

b. Docking interaction compounds identified through GC-MS analysis against DNA gyrase

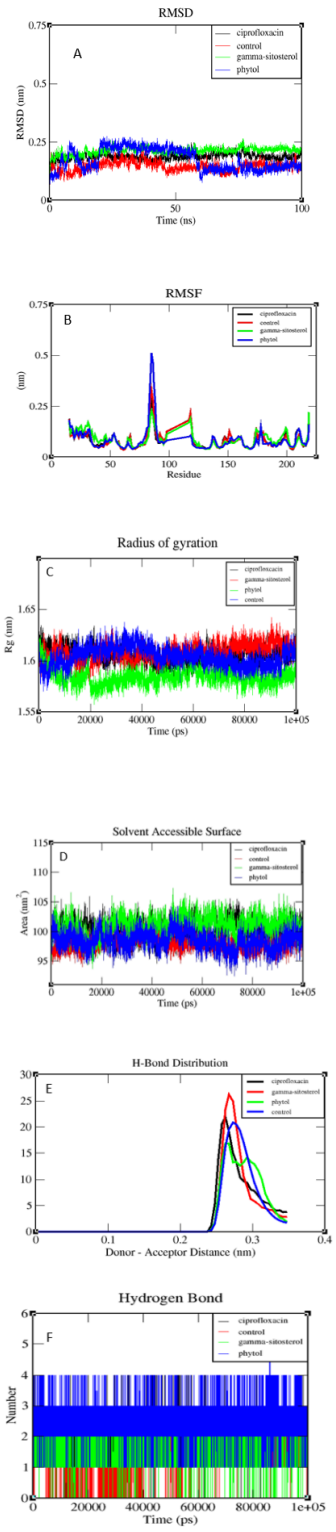

Figure 6

Plot of MD simulation between protein DNA gyrase (control) and ligands are (ciprofloxacin, gamma-sitosterol and phytol). (A) RMSD (B) RMSF (C) Radius of gyration (D) SASA (E) H-bond distribution (F) H bond number.

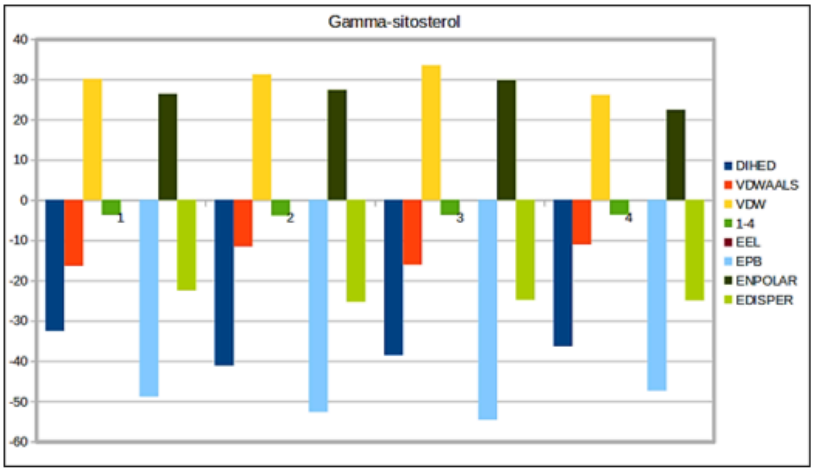

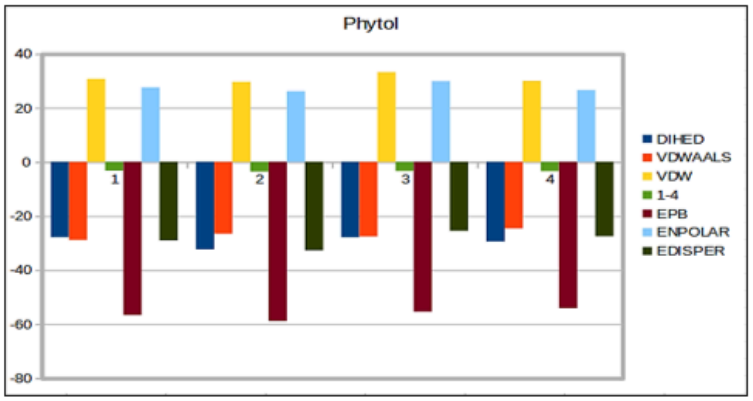

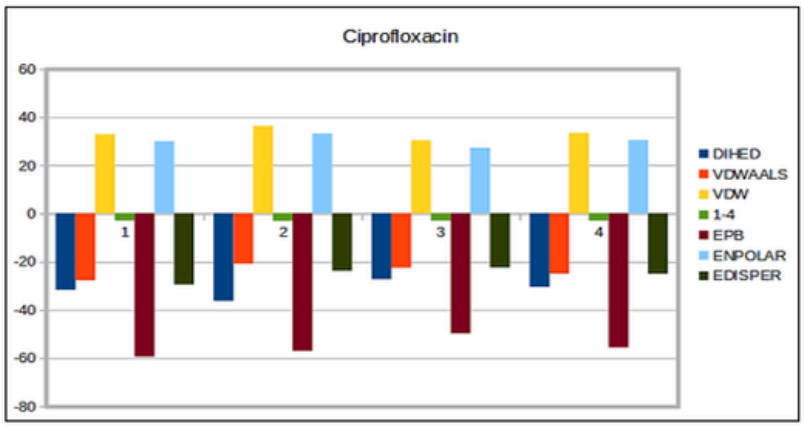

Figure 7

Diagrammatic representation of protein–ligand complexes through MM-PBSA analysis

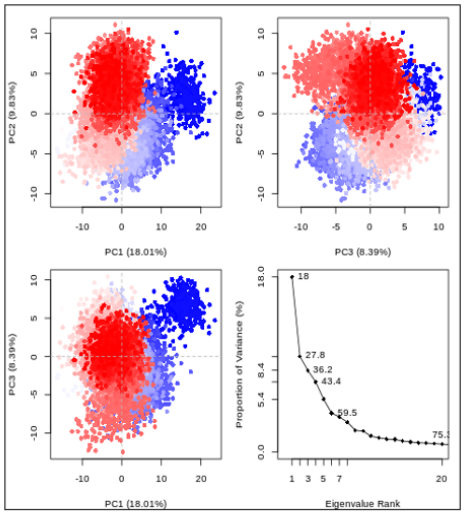

Fig. 8 a.

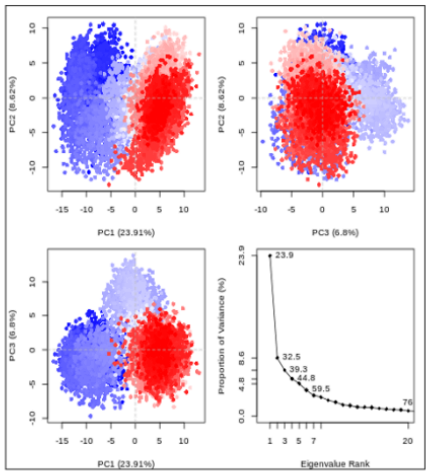

Fig. 8 b

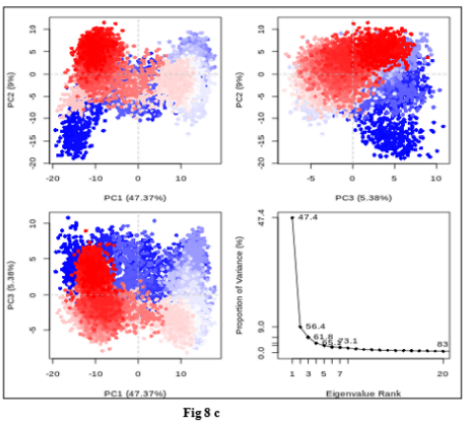

Fig 8 c

Figure 8

a. Ciprofloxacin

b. Gamma sitosterol

c. Phytol